Kinetics of the CH_3O_2 + NO Reaction: Temperature Dependence of the Overall Rate Constant and an Improved Upper Limit for the CH_3ONO_2 Branching Channel

Kurtis W. Scholtens, Benjamin M. Messer, Christopher D. Cappa, and Matthew J. Elrod*

Department of Chemistry, Hope College, Holland, MI, 49423

Received: February 8, 1999; In Final Form: April 12, 1999

The overall rate constant and an upper limit for the CH_3ONO_2 product channel for the CH_3O_2 + NO reaction have been measured using the turbulent flow technique with high-pressure chemical ionization mass spectrometry for the detection of reactants and products. At room temperature and 100 Torr pressure, the rate constant (and the two standard deviation error limit) was determined to be $(7.8 \pm 2.2) \times 10^{-12}$ cm^3 molecule^{-1} s^{-1}. The temperature dependence of the rate constant was investigated between 295 and 203 K at pressures of either 100 or 200 Torr, and the data was fit to the following Arrhenius expression: $(9.2^{+6.0}_{-3.9} \times 10^{-13})$ exp[$(600 \pm 140)/T$] cm^3 molecule^{-1} s^{-1}. Although the room-temperature rate constant value agrees well with the current recommendation for atmospheric modeling, our values for the rate constant at the lowest temperatures accessed in this study (203 K) are about 50% higher than the same recommendation. No CH_3ONO_2 product was detected from the CH_3O_2 + NO reaction (using direct CH_3ONO_2 detection methods for the first time), but an improved upper limit of 0.03 (at 295 K and 100 torr) for this branching channel was determined.

Introduction

The methylperoxy radical (CH_3O_2) is an important intermediate species formed in the oxidation of methane in the atmosphere.

$$CH_4 + OH \rightarrow CH_3 + H_2O \quad (1)$$

$$CH_4 + O(^1D) \rightarrow CH_3 + OH \quad (2)$$

$$CH_3 + O_2 + M \rightarrow CH_3O_2 + M \quad (3)$$

Ozone levels in the atmosphere are directly affected by CH_3O_2 reactions, which themselves are dependent on the levels of the nitrogen oxides (NO_x). Under high NO_x conditions (generally, lower tropospheric urban conditions), CH_3O_2 reactions lead to the production of ozone, the most deleterious constituent of photochemical smog.

$$CH_3O_2 + NO \rightarrow CH_3O + NO_2 \quad (4a)$$

$$NO_2 + h\nu\ (\lambda < 380\ \text{nm}) \rightarrow NO + O \quad (5)$$

$$O + O_2 + M \rightarrow O_3 + M \quad (6)$$

CH_3O_2 can also be temporarily removed from the ozone production cycles by the formation of reservoir species.

$$CH_3O_2 + NO + M \rightarrow CH_3ONO_2 + M \quad (4b)$$

$$CH_3O_2 + NO_2 + M \rightarrow CH_3O_2NO_2 + M \quad (7)$$

$$CH_3O_2 + HO_2 \rightarrow CH_3OOH + O_2 \quad (8)$$

A potential product of reaction 4, methyl nitrate (CH_3ONO_2), has been directly measured in the atmosphere and suggested as a tracer of the photochemical age of air masses,[1] but the chemical processes leading to its presence in the atmosphere remain unclear.[2] Recently, Wennberg et al.[3] reported the measurement of higher HO_x levels than predicted in the upper troposphere of the northern hemisphere. Because this result suggests that this region of the atmosphere is not ordinarily dominated by NO_x chemistry, it is therefore more susceptible to anthropogenic NO_x emissions than previously thought. This is an important finding since it indicates that increased air traffic in the upper troposphere may lead to a substantial increase in ozone levels. Therefore, it is critical to obtain the relative rates of reactions 4, 7, and 8 and to determine the product distributions of these reactions in order to address the impact of CH_3O_2 chemistry on this issue.

The CH_3O_2 + NO reaction has received considerable study[4−10] because of its important role in the formation of tropospheric ozone. In the most recent study, Villalta et al.[11] used low-pressure chemical ionization mass spectrometry (CIMS) to measure the negative temperature dependence of the rate constant to temperatures as low as 200 K. Although this study included temperatures of the upper troposphere, the experiments were carried out at low pressure (∼ 3 Torr). Because of this limitation, Villalta et al. suggested that under the actual high-pressure and low-temperature conditions of the upper troposphere that the association reaction (channel 4b) could not be ruled out as an important source of methyl nitrate. Previously, there had been two studies of the product branching channels for reaction 4 at 298 K, and in neither case was evidence found for branching into channel 4b. Ravishankara et al. established an upper limit branching ratio $[k_{4b}/(k_{4a} + k_{4b})]$ of 0.24 for channel 4b by following the production of the channel 4a product, NO_2, and applying mass balance arguments to determine the maximum branching into channel 4b that was consistent with the data.[6] Zellner et al. determined an upper limit of 0.20 for channel 4b by following the production of the other channel 4a product, CH_3O, and again applying mass

* Corresponding author. E-mail: elrod@hope.edu. Phone: (616) 395-7629. Fax: (616) 395-7118.

10.1021/jp990469k CCC: $18.00
Published on Web 05/14/1999

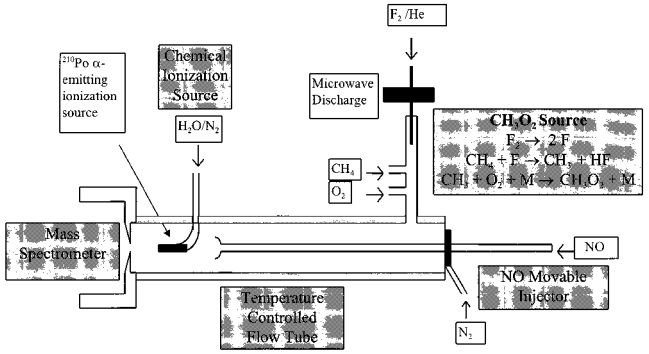

Figure 1. Experimental apparatus.

balance arguments to determine the maximum branching into channel 4b that was consistent with their data.[9] In addition, Atkinson and co-workers have developed an empirical relationship for the yield of organic nitrates from environmental chamber photolysis studies of C_3-C_9 hydrocarbon/NO mixtures at 298 K.[12] Although this relationship probably provides only a qualitative estimate of potential methyl nitrate formation from reaction 4, it is important to note that the branching ratio is predicted to rise from 0.005 for the methyl case to 0.16 for the *n*-heptyl case at 298 K and 760 torr, thus indicating the importance of the association channel for the larger alkyl peroxy radicals.

In this article we describe our investigation of the kinetics of the CH_3O_2 + NO reaction conducted at pressures at 100 and 200 Torr and at a range of temperatures extending to those found in the lower stratosphere using a turbulent flow (TF) tube coupled to a high-pressure chemical ionization mass spectrometer (CIMS). It has been previously shown that TF technique can be used to accurately determine the rate constants of reactions at pressures ranging from 50 to 760 Torr and at temperatures as low as 180 K.[13] As in previous kinetics studies of HO_2 + NO (ref 14), HO_2 + BrO (ref 15), and OH + ClO (ref 16) using the coupled TF−CIMS approach, we are able to directly access atmospheric pressure and temperature conditions and sensitively monitor many of the relevant reactants and products for the CH_3O_2 + NO reaction. In the OH + ClO work mentioned above, the CIMS detection methodology allowed for the first identification of a minor HCl-producing channel for the OH + ClO reaction, thus resolving a long-standing inconsistency between predicted and measured stratospheric HCl concentrations.[16] In this work, we describe our development of a new chemical ionization detection scheme for CH_3ONO_2, which allows for the first direct product study of reaction channel 4b.

Experimental Section

Turbulent Fast Flow Kinetics. A schematic of the experimental apparatus is presented in Figure 1 and is similar to that used in a previous study of HO_2 + NO (ref 14). The flow tube was constructed with 2.2 cm i.d. Pyrex tubing and was 100 cm in total length. A large flow of nitrogen carrier gas (approximately 30 STP L min^{-1}) was injected at the rear of the flow tube. The gases necessary to generate CH_3O_2 were introduced through a 10 cm long 12.5 mm diameter sidearm located at the rear of the flow tube. NO was added via an encased movable injector. The encasement (made from corrugated Teflon tubing) was used so that the injector could be moved to various injector positions without breaking any vacuum seals, as well as to prevent ambient gases from condensing on cold portions of the injector. A fan-shaped Teflon device was placed at the end of the injector in order to enhance turbulent mixing. The polonium-210 α-emitting ionization source was placed between the temperature regulated flow tube and the inlet to the quadrupole mass spectrometer. All gas flows were monitored with calibrated mass flow meters. The flow tube pressure was measured upstream of the ionization source using a 0−1000 Torr capacitance manometer. The temperature was determined at both the entrance and exit points of the temperature regulated region of the flow tube using Cu−constantan thermocouples.

Reactant Preparation. CH_3O_2 was generated using the following reactions:

$$CH_4 + F \rightarrow CH_3 + HF \quad (9)$$

$$CH_3 + O_2 + M \rightarrow CH_3O_2 + M \quad (10)$$

($k_9 = 6.7 \times 10^{-11}$ cm^3 $molecule^{-1}$ s^{-1} and $k_{10} = 4.9 \times 10^{-13}$ cm^3 $molecule^{-1}$ s^{-1} at 100 Torr).[17] Fluorine atoms were produced by passing a dilute F_2/He mixture through a microwave discharge produced by a Beenakker cavity operating at 50 W. The dilute F_2/He mixture was obtained by combining a 2.0 STP L min^{-1} flow of helium (99.999%), which had passed through a silica gel trap immersed in liquid nitrogen, with a 0.5−5.0 STP mL min^{-1} flow of a 1% F_2/He mixture (Excimer grade). To generate CH_3, the fluorine atoms were then injected into a sidearm and mixed with an excess of CH_4 (CP grade, $\sim 10^{15}$ molecule cm^{-3}) in order to ensure that no fluorine atoms were introduced into the main flow. CH_3O_2 was then produced by the addition of a large excess of O_2 (99.995%; $\sim 5 \times 10^{17}$ molecule cm^{-3}) just downstream of the production of CH_3. Absolute CH_3O_2 concentrations (needed to ensure pseudo-first-order kinetics conditions and for branching ratio modeling) were determined by the titration reactions

$$CH_3O_2 + NO \rightarrow CH_3O + NO_2 \quad (11)$$

$$CH_3O + O_2 \rightarrow CH_2O + HO_2 \quad (12)$$

($k_{11} = 7.8 \times 10^{-12}$ cm^3 $molecule^{-1}$ s^{-1} and $k_{12} = 1.9 \times 10^{-15}$ cm^3 $molecule^{-1}$ s^{-1})[17] and subsequent calibration of the CH_2O mass spectrometer signal. Computer modeling of these titration reactions indicates that not all of the CH_3O_2 initially present is converted to the stable species, CH_2O. This is mainly due to reactions of CH_3O with other species in the chemical system (which will be addressed in the discussion section). Therefore, the CH_3O_2 concentrations were calculated from the CH_2O concentrations by explicitly determining the conversion factor (usually ~0.7) from computer modeling for the specific experimental conditions. The NO (CP grade) used in reaction 11 was purified by several freeze/pump/thaw cycles to remove NO_2 impurities. The NO_2/NO ratio of the purified sample was typically less than 1% as determined from CIMS NO_2 detection and calibration methods. The standard CH_2O samples required for calibration of the mass spectrometer signal were prepared by heating paraformaldehyde and trapping the gaseous product. For this study, CH_3O_2 concentrations ranged from 0.5 to 15.0 $\times 10^{11}$ molecule cm^{-3}.

For the actual kinetics experiments, NO was purified before use as described above and was added to the flow reactor as a 10% mixture in N_2 through the movable injector. NO concentrations used in this study ranged from 0.5 to 20.0 $\times 10^{12}$ molecule cm^{-3}. To ensure pseudo-first-order kinetics conditions, [NO] was kept more than 10 times larger than [CH_3O_2].

For the low-temperature studies, liquid nitrogen cooled silicone oil was used as the coolant for the jacketed flow tube.

Nitrogen carrier gas was precooled by passing it through a copper coil immersed in a liquid N_2 reservoir followed by resistive heating. The temperature was controlled in the reaction region to within 1 K.

CH_3ONO_2 Branching Channel Measurements. In these studies, the potential production of CH_3ONO_2 from reaction 4b was monitored directly over a reaction time of ~25 ms. Because no CH_3ONO_2 product was actually observed, computer modeling was used to determine an upper limit for the rate constant of reaction 4b. The method involved using the initial measured concentrations of CH_3O_2, NO, and all precursors and then determining the largest rate constant (k_{4b}) for which CH_3ONO_2 production would remain below the detection level of the mass spectrometric analytical method (defined as a signal-to-noise ratio of 2:1). For these experiments, higher CH_3O_2 levels were used than in the determination of the bimolecular rate constant (to increase the concentration of the potential product). A side reaction resulting from the reaction of the products of the main channel (4a) of reaction 4,

$$CH_3O + NO_2 + M \rightarrow CH_3ONO_2 + M \qquad (13)$$

($k_{13} = 1.2 \times 10^{-11}$ cm^3 molecule^{-1} s^{-1} at 100 Torr),[17] is a potential source of CH_3ONO_2, and experimental conditions must be designed to minimize this reaction. By keeping O_2 concentrations very high, reaction 12 will consume most of the CH_3O produced by reaction 4a and minimize production of CH_3ONO_2 by reaction 13.

To determine the detection sensitivity of the mass spectrometer for CH_3ONO_2, standard samples of CH_3ONO_2 were prepared. CH_3ONO_2 was prepared by dropwise addition of a solution of 5 mL of 95% H_2SO_4 and 15 mL of reagent grade CH_3OH to an ice-bath cooled solution containing 30 mL of 95% H_2SO_4 and 30 mL of 70% HNO_3. The resulting solution was transferred to a separatory funnel, and the lower layer (acid) was drained off. The organic layer (containing CH_3ONO_2) was then washed several times with a 22% NaCl solution, which was stored in a refrigerated flask. The high purity of the CH_3ONO_2 sample was confirmed by FTIR spectroscopy, and the samples did not undergo degradation over the course of several weeks. Standard samples were prepared by drawing an appropriate amount of CH_3ONO_2 vapor from the liquid sample and mixing with N_2 to make 1% CH_3ONO_2 mixtures appropriate for mass spectrometric calibration.

Chemical Ionization Mass Spectrometric Detection. A positive ion chemical ionization scheme (with H_3O^+ as the reagent ion) was used to detect CH_3O_2 and CH_2O, and a negative chemical ionization scheme (F^-) was used to detect CH_3ONO_2 with the quadrupole mass spectrometer. H_3O^+ was produced in the ion source by passing a large O_2 flow (10 STP L min^{-1}) through the polonium-210 α-emitting ionization source (with H_2O impurities being sufficiently abundant to produce adequate quantities of reagent ions). F^- was produced in the ion source by passing a large N_2 flow (10 STP L min^{-1}) and 0.1 STP mL min^{-1} of NF_3 through the ionization source. The commercial ionization source consisted of a hollow cylindrical (69 by 12.7 mm) aluminum body with 10 mCurie (3.7×10^8 disintegrations/s) of polonium-210 coated on the interior walls.

Ions were detected with a quadrupole mass spectrometer housed in a two-stage differentially pumped vacuum chamber. Flow tube gases (neutrals and ions) were drawn into the front chamber through a 0.1 mm aperture, which was held at a potential of ±210 V. The ions were focused by three lenses constructed from 3.8 cm i.d., 4.8 cm o.d aluminum gaskets. The front chamber was pumped by a 6 in. 2400 L s^{-1} diffusion pump. The gases entered the rear chamber through a skimmer cone with a 1.0 mm orifice (held at ±130 V) which was placed approximately 5 cm from the front aperture. The rear chamber was pumped by a 250 L s^{-1} turbomolecular pump. Once the ions passed through the skimmer cone, they were mass filtered and detected with a quadrupole mass spectrometer.

Chemical Ionization Schemes. To perform pseudo-first-order kinetics studies of the overall rate constant of reaction 4, a chemical ionization scheme for the CH_3O_2 reactant is required. Villalta et al.[11] developed the following chemical ionization scheme for CH_3O_2:

$$CH_3O_2 + O_2^+ \rightarrow CH_3O_2^+ + O_2 \qquad (14a)$$

$$CH_3O_2 + O_2^+ \rightarrow CH_3^+ + O_2 + O_2 \qquad (14b)$$

They found that the fragmentation reaction 14b was the predominant (75%) channel for ionization by O_2^+. Although it is somewhat unusual to observe fragmentation in chemical ionization processes, the fragmentation observed in this process is easily explained by the very large difference in ionization potentials for O_2 [12.07 eV (ref 18)] and CH_3O_2 [7.36 eV (ref 19)]. The relatively large exothermicity of this charge-transfer process (454 kJ mol^{-1}) drives the dissociation of $CH_3O_2^+$ cation. Villalta et al. were able to overcome the fragmentation problem in their study by careful calibration of the CH_3^+ signal. However, we sought to find a less exothermic chemical ionization process for our work with CH_3O_2. In another study, we have undertaken extensive ab initio G2-level electronic structure and thermodynamics studies of the HOOH and CH_3-OOH neutral and ionic species as part of the development of chemical ionization mass spectrometric detection methods for peroxides.[20] From this work, we identified the following chemical ionization scheme for CH_3O_2:

$$CH_3O_2 + H_3O^+ \rightarrow CH_3OOH^+ + H_2O \qquad (15)$$

The calculated exothermicity of this reaction is only 25 kJ mol^{-1} (because of the very similar proton affinities of CH_3O_2 and H_2O), thus ensuring the stability of the ionic product CH_3OOH^+. This chemical ionization detection scheme was experimentally tested, and reaction 15 was found to be sufficiently fast to serve as a sensitive method for the detection of CH_3O_2. Depending on the amount of the water in the flow system, CH_3O_2 was detected as $CH_3OOH^+(H_2O)_n$, where n was typically 2 or 3.

To perform branching ratio measurements for reaction 4b, chemical ionization schemes are needed for CH_2O (for CH_3O_2 absolute concentration determinations) and CH_3ONO_2. In a previous study, formaldehyde was found to react quickly with H_3O^+,

$$CH_2O + H_3O^+ \rightarrow CH_2OH^+ + H_2O \qquad (16)$$

($k_{16} = 3 \times 10^{-9}$ cm^3 molecule^{-1} s^{-1}).[21] Again, depending on the amount of the water in the flow system, CH_2O was detected as $CH_2OH^+(H_2O)_n$, where n was typically 2 or 3. The third species for which a chemical ionization scheme must be developed is CH_3ONO_2. Recent experimental[22] and theoretical[23] studies have definitively shown that CH_3ONO_2 has a larger proton affinity than water, suggesting that CH_3ONO_2 can also be detected with H_3O^+.

$$CH_3ONO_2 + H_3O^+ \rightarrow CH_3ONO_2 \cdot H^+ + H_2O \qquad (17)$$

However, we found that our experimental sensitivity using this

reaction for the detection of CH_3ONO_2 was not sufficient for branching ratio studies. Presumably, this result is due to a relatively slow rate constant for reaction 17. Interestingly, Lee and Rice have predicted that the proton actually bonds to the bridging oxygen atom rather than the terminal oxygen atoms.[23] Thus, the fraction of reactive orientations achieved by collisions of H_3O^+ and CH_3ONO_2 molecules may be sterically limited and may help explain why reaction 17 is relatively slow. In work to be published,[24] we investigated several potential chemical ionization schemes for CH_3ONO_2 with ab initio G2-level electronic structure and thermodynamics calculations and found the following reaction to be exothermic.

$$CH_3ONO_2 + F^- \rightarrow CH_3ONO_2 \cdot F^- \qquad (18)$$

Upon experimental testing of the above ionization scheme, it was found that reaction 18 provided sufficient sensitivity for the branching ratio studies. The electronic structure calculations indicate that the fluoride atom bonds with one of the methyl hydrogen atoms. Again, depending on the amount of the water in the flow system, CH_3ONO_2 was detected as $CH_3ONO_2 \cdot F^-(H_2O)_n$, where n was typically 2 or 3.

Results and Discussion

Detection Sensitivity. In earlier kinetics work with TF−CIMS methodology, it was reported that various negative ion chemical ionization detection schemes resulted in sensitivities of 100, 200, and 1000 ppt (at 100 Torr) for NO_2, HO_2, and OH, respectively.[14] As part of the branching ratio measurements, we carried out formal calibrations of the mass spectrometer for CH_3O_2, CH_2O, and CH_3ONO_2. It was apparent that these species (detected in both negative and positive ion mode) could be detected with similar sensitivity to that obtained for the species listed above, thus demonstrating the generality of the CIMS technique. The mass spectrometer signals for these compounds were found to be linear over the range of concentrations used in this work. The stated sensitivity was more than adequate for the present work; actually, it was necessary to degrade the sensitivity of the spectrometer (by decreasing the ion−molecule reaction time) to allow the introduction of greater amounts of reactants. This was necessary in order to study the relatively slow CH_3O_2 + NO reaction without inducing complications from secondary ion−molecule processes.

Rate Constant Determination. Bimolecular rate constants were obtained via the usual pseudo-first-order approximation method, using NO as the excess reagent. Typical CH_3O_2 decay curves as a function of injector distance are shown in Figure 2. The first-order rate constants obtained from fitting the CH_3O_2 decay curves were plotted against NO in order to determine the bimolecular rate constant, as shown in Figure 3. This approach for determining bimolecular rate constants assumes that deviations from the plug flow approximation (molecular velocities are equal to the bulk flow velocity) are negligible. Under the conditions present in our turbulent flow tube (Reynolds number > 2000), Seeley et al. estimated that these deviations result in apparent rate constants which are at most 8% below the actual values.[25] Hence, the flow corrections were neglected as they are smaller than the sum of the other likely systematic errors in the measurements of gas flows, temperature, detector signal, and pressure. Considering such sources of error, we estimate that rate constants can be determined with an accuracy of ±30% (2σ).

We performed three separate determinations of the rate constant at 100 Torr and 295 K (see Table 1 for a complete list of experimental conditions and measured rate constants) and arrived at the mean value of $k = (7.8 \pm 2.2) \times 10^{-12}$ cm^3 molecule^{-1} s^{-1}; the uncertainty represents the two standard deviation statistical error in the data and is not an estimate of systematic errors. Table 2 contains a comparison of all reported

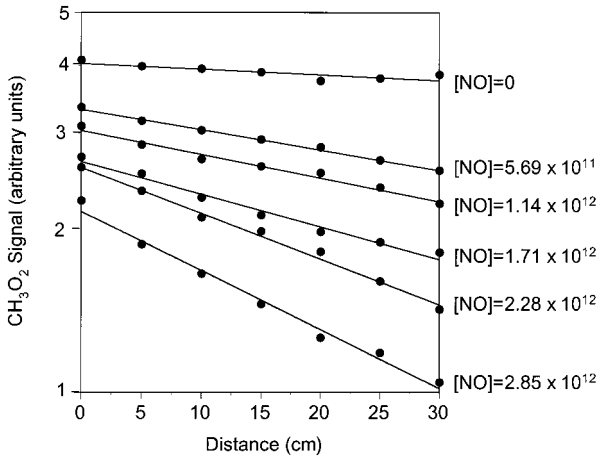

Figure 2. Pseudo-first-order CH_3O_2 decay curves for the CH_3O_2 + NO reaction at 200 Torr, 295 K, and 960 cm s^{-1} velocity (NO concentrations in molecule cm^{-3}).

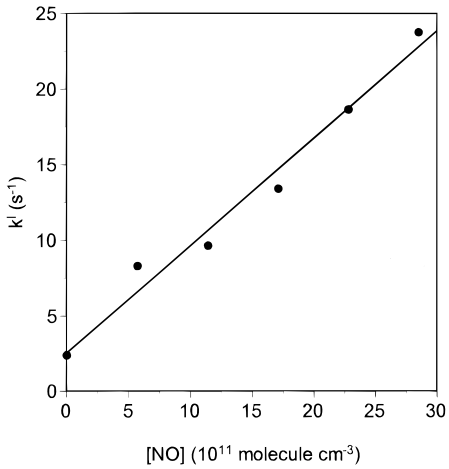

Figure 3. Determination of bimolecular rate constant for the CH_3O_2 + NO reaction from data in Figure 2.

TABLE 1: CH_3O_2 + NO Temperature and Pressure Dependence Data

temperature (K)	pressure (Torr)	velocity (cm s^{-1})	Reynolds number	k_4[a] (10^{-12} cm^3 molecule^{-1} s^{-1})
295	100	1240	2200	6.5 ± 1.9
295	100	1240	2200	8.5 ± 1.3
295	100	1200	2300	8.3 ± 1.6
295	200	960	3700	7.1 ± 1.1
273	200	930	3700	7.3 ± 0.9
263	100	1060	2300	8.2 ± 2.6
248	100	1240	2800	12.2 ± 3.5
243	100	1020	2200	9.2 ± 3.0
238	200	800	4100	8.5 ± 2.5
233	100	1120	3400	10.5 ± 3.6
228	100	1000	2400	15.4 ± 4.7
223	100	1100	3200	11.4 ± 3.8
218	100	900	2800	13.5 ± 6.2
218	100	1000	2400	15.8 ± 5.5
213	100	950	2780	18.1 ± 4.0
213	200	810	4100	15.6 ± 4.5
208	100	925	3255	17.6 ± 5.9
203	100	890	3444	18.3 ± 4.0

[a] Errors are 2σ.

TABLE 2: Selected Pressure- and Temperature-Dependent Results from Kinetics Studies of the CH_3O_2 + NO Reaction

study	temperature (K)	pressure (Torr)	k_4 (10^{-12} cm^3 molecule^{-1} s^{-1})
Simonaitis and Heicklen[7]	296	~100	7.7
	218	~200	13.5
Ravishankara et al.[6]	298	100	7.5
Villalta et al.[11]	298	2−5	7.5
	218	2−5	10.0[a]
this work	295	100	7.8
	218	100	14.4[a]

[a] Values calculated from fitted Arrhenius expressions.

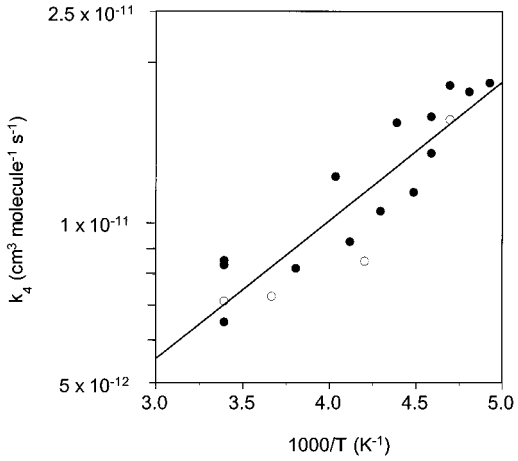

Figure 4. Arrhenius plot of the temperature dependence of the rate constant for the CH_3O_2 + NO reaction determined in this work: (●) 100 Torr; (○) 200 Torr.

rate constants for the CH_3O_2 + NO reaction near room temperature and at 218 K for the studies in which the temperature dependence was investigated. Our room-temperature rate constant is in excellent agreement with previous studies and thus with the JPL recommended value for atmospheric modeling.[17]

Temperature Dependence of the Rate Constant. We performed several measurements at temperatures between 295 and 203 K in order to establish the temperature dependence of the rate constant for conditions relevant to the upper troposphere (and lower stratosphere). The rate constant approximately doubled as the temperature was lowered over this range. From the data listed in Table 1 and plotted in Figure 4, we obtain the Arrhenius expression $k(T) = (9.2^{+6.0}_{-3.9} \times 10^{-13}) \exp[(600 \pm 140)/T]$ cm^3 molecule^{-1} s^{-1}. There have been three previous studies of the temperature dependence of this reaction. Two relatively high-pressure (~ 100 Torr) studies by Simonaitis and Heicklen[7] and Ravishankara et al.[6] at a few selected temperatures and a thorough low-pressure (~3 Torr) study by Villalta et al.[11] (which allowed a similar Arrhenius analysis to that described above for our study at 100 Torr) have been performed for this reaction. In Table 2, the rate constants determined from the previous temperature-dependent work and this work are compared at a temperature of 218 K (which is one of the temperatures included in the Simonaitis and Heicklen work; the rate constants at 218 K for the Villalta et al. study and this work are calculated from the appropriate Arrhenius expressions). It is apparent that the rate constant determined in this study at 218 K is more consistent with the Simonaitis and Heicklen value than with the Villalta et al. value. It is important to note that the Villalta et al. 218 K rate constant is within the 2σ error limit of our calculated 218 K rate constant. However, our analysis does indicate a statistically significant larger temperature dependence (exp[(600 ± 140)/T]) for the rate constant than in the Villalta et al. analysis (exp[(285 ± 60)/T]). In Figure 5 we present Arrhenius plots for all four temperature-dependent studies. It is apparent that all four studies are in good agreement at temperatures above 250 K, but our work and that of Simonaitis and Heicklen indicate a faster rate constant at temperatures below 250 K.

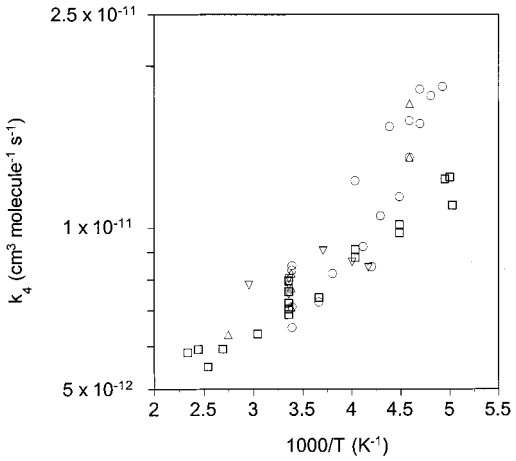

Figure 5. Arrhenius plot of all temperature-dependent data for the CH_3O_2 + NO reaction: (○) this work; (□) ref 11; (△) ref 7; (▽) ref 6.

Pressure Dependence. Because of the disagreement between the low-pressure and high-pressure studies of the low-temperature rate constant for the CH_3O_2 + NO reaction, it is possible that the rate constant has a greater pressure-dependent component at low temperatures. Due to the negative Arrhenius behavior of the overall rate constant, it is reasonable to assume that the reaction proceeds through an intermediate in the following fashion:

$$CH_3O_2 + NO \leftrightarrow [CH_3OONO]^* \rightarrow CH_3O + NO_2 \quad (19)$$
$$\downarrow[M]$$
$$CH_3ONO_2 \quad (20)$$

The possibility of a increased pressure-dependent component to the rate constant is reasonable given that the lower temperatures should increase the lifetime of the $[CH_3OONO]^*$ collisional intermediate complex. It is then possible that an increase in total pressure from 3 to 100 Torr would increase the rate of collisional stabilization of the energized intermediate by the bath gas and thus increase the lifetime of the $[CH_3OONO]^*$ complex further. This, in turn, would lead to a higher proportion of $[CH_3OONO]^*$ collisional pairs going on to form products (either CH_3O + NO_2 or CH_3ONO_2) and thus result in a higher measured rate constant. To explore this potential effect, we investigated the rate constant at an increased pressure of 200 Torr at temperatures of 295, 273, 238, and 213 K. We did not observe any significant difference in the temperature dependence of the rate constant compared to our studies at 100 Torr, so the 200 Torr data was included in the Arrhenius analysis described above. However, since our work covers a relatively narrow pressure range, these results are not conclusive concerning the possibility of a pressure-dependent component to the rate constant. Therefore, it is important to emphasize that the low-pressure results of Villalta et al., the high-pressure results of Simonaitis and Heicklen, and those presented here may be reconciled by the existence of a pressure-dependent component to the rate constant which is greater at lower temperatures.

CH_3ONO_2 Branching Ratio Determination. We performed several measurements aimed at establishing a value for the CH_3-

TABLE 3: Chemical Reactions Used in Kinetics Modeling for Branching Ratio Determination

reaction	k (cm^3 $molecule^{-1}$ s^{-1}) at 295 K, 100 Torr[a]
$CH_3O_2 + NO \rightarrow CH_3O + NO_2$	7.0×10^{-12}
$CH_3O_2 + CH_3O_2 \rightarrow 2CH_3O + O_2$	1.4×10^{-13}
$CH_3O_2 + CH_3O_2 \rightarrow CH_2O + CH_3OH + O_2$	2.8×10^{-13}
$CH_3O_2 + NO_2 \rightarrow CH_3O_2NO_2$	1.8×10^{-12}
$CH_3O + NO \rightarrow CH_3ONO$	1.3×10^{-11}
$CH_3O + NO_2 \rightarrow CH_3ONO_2$	1.2×10^{-11}
$CH_3O + O_2 \rightarrow CH_2O + HO_2$	1.8×10^{-15}
$HO_2 + NO \rightarrow OH + NO_2$	8.2×10^{-12}
$OH + NO \rightarrow HONO$	1.8×10^{-12}
$OH + HO_2 \rightarrow H_2O + O_2$	1.1×10^{-10}
$OH + OH \rightarrow H_2O_2$	1.9×10^{-12}
$OH + NO_2 \rightarrow HNO_3$	3.5×10^{-12}
$OH + CH_2O \rightarrow H_2O + HCO$	1.0×10^{-11}

[a] From ref 17.

TABLE 4: Branching Ratio Measurement Conditions and Analysis

parameter	value
pressure (Torr)	100
temperature (K)	295
initial observation time (ms)	20
final observation time (ms)	47
initial [CH_3O_2] (molecule cm^{-3})	1.43×10^{12}
initial [NO] (molecule cm^{-3})	1.75×10^{13}
initial [O_2] (molecule cm^{-3})	5.0×10^{17}
[CH_3ONO_2] (molecule cm^{-3}) resulting from $CH_3O + NO_2$ reaction	2.8×10^{9}
minimum detectable [CH_3ONO_2] (molecule cm^{-3})	3.3×10^{9}
upper limit for k_{4b} (cm^3 $molecule^{-1}$ s^{-1}) determined from kinetics conditions and kinetic modeling	2.0×10^{-13}

TABLE 5: Results from Direct Branching Ratio Studies of the CH_3O_2 + NO Reaction

study	product monitored	temperature (K)	pressure (Torr)	$k_{4b}/(k_{4a} + k_{4b})$
Ravishankara et al.[6]	NO_2	298	40	<0.24
Zellner et al.[9]	CH_3O	298	8	<0.20
this work	CH_3ONO_2	295	100	<0.03

ONO_2 branching ratio [$k_{4b}/(k_{4a} + k_{4b})$]. These measurements were performed with much higher sensitivity than previous efforts because the CH_3ONO_2 product was directly monitored by the CIMS method described above. Table 3 lists the chemical reactions and relevant rate constants used in the kinetics modeling to determine the experimental upper limit for the CH_3ONO_2 branching ratio. Table 4 lists a typical set of experimental conditions, maximum predicted [CH_3ONO_2] produced from the side reaction $CH_3O + NO_2$ (reaction 13), and the overall CH_3ONO_2 detection sensitivity for the branching ratio measurement (defined as a signal/noise ratio of 2:1). As can be seen from this table for these experimental conditions, the amount of CH_3ONO_2 produced from reaction 13 is roughly equal to the detection level for CH_3ONO_2. Thus, the ultimate lower limit on the value for the branching ratio for reaction 4b is constrained by *both* the secondary chemistry from reaction 13 and the sensitivity level of the analytical method used here. None of our branching ratio experiments indicated the production of CH_3ONO_2 from the CH_3O_2 + NO reaction. However, we were able to determine a much improved upper limit for $k_{4b}/(k_{4a} + k_{4b})$ of 0.03 at 295 K and 100 Torr. Table 5 compares the previously indirectly determined upper limits for $k_{4b}/(k_{4a} + k_{4b})$ with the value determined here. It is clear that our value for $k_{4b}/(k_{4a} + k_{4b})$ places a much tighter constraint on the amount of CH_3ONO_2 that can be formed from the CH_3O_2 + NO reaction. Because our temperature-dependent results for the overall rate constant indicate the possibility of a low-temperature pressure-dependent channel and CH_3ONO_2 production would be expected to be maximized under these conditions, we attempted to investigate the temperature dependence of the branching ratio. However, reduced CIMS sensitivity for CH_3ONO_2 at the lower temperatures precluded the determination of a comparably good upper limit as that obtained at 295 K.

Conclusions

The results presented here extend the measurements of the overall rate constant for CH_3O_2 + NO reaction to the temperature *and* pressure conditions representative of the upper troposphere and lower stratosphere. Although our value for the room temperature rate constant agrees well with the current recommendation for stratospheric modeling, our values for the rate constant at the lowest temperatures attained in this study (203 K) are about 50% higher than the same recommendation, which was largely determined from low-pressure measurements (~3 Torr). However, our low-temperature results are in agreement with previous studies at similar pressure (~100 Torr), suggesting the possibility of an increased pressure-dependent component to the rate constant at low temperature. No CH_3ONO_2 product was detected (using CH_3ONO_2 specific detection methods for the first time) from the CH_3O_2 + NO reaction, but an improved upper limit of 0.03 (at 295 K and 100 torr) for this branching channel [$k_{4b}/(k_{4a} + k_{4b})$] was determined.

Acknowledgment. This research was funded by grants from the Camille and Henry Dreyfus Foundation, American Chemical Society−Petroleum Research Fund, Research Corporation, the Michigan Space Grant Consortium, and the National Science Foundation.

References and Notes

(1) Bertman, S. B.; Roberts, J. M.; Parrish, D. D.; Buhr, M. P.; Goldan, P. D.; Kuster, W. C.; Fehsenfeld, F. C.; Montzka, S. A.; Westberg, H. *J. Geophys. Res.* **1995**, *100*, 22805.

(2) Flocke, F.; Atlas, E.; Madronich, S.; Schauffler, S. M.; Aikin, K.; Margitan, J. J.; Bui, T. P. *Geophys. Res. Lett.* **1998**, *25*, 1891.

(3) Wennberg, P. O.; Hanisco, T. F.; Jaeglé, L.; Jacob, D. J.; Hintsa, E. J.; Lanzendorf, E. J.; Anderson, J. G.; Gao, R.; Keim, E. R.; Donnelly, S. G.; Negro, L. A.; Fahey, D. W.; McKeen, S. A.; Salawitch, R. J.; Webster, C. R.; May, R. D.; Herman, R. L.; Proffitt, M. H.; Margitan, J. J.; Atlas, E. L.; Schauffler, S. M.; Flocke, F.; McElroy, C. T.; Bui, T. P. *Science* **1998**, *279*, 49.

(4) Cox, R. A.; Tyndall, G. S. *Chem. Phys. Lett*. **1979**, *65*, 357.

(5) Sander, S. P.; Watson, R. T. *J. Phys. Chem*. **1980**, *84*, 1664.

(6) Ravishankara, A. R.; Eisele, F. L.; Kreutter, N. M.; Wine, P. H. *J. Chem. Phys.* **1981**, *74*, 2267.

(7) Simonaitis, R.; Heicklen, J. *J. Phys. Chem*. **1981**, *85*, 2946.

(8) Plumb, I. C.; Ryan, K. R.; Steven, J. R.; Mulcahy, M. F. R. *J. Phys. Chem*. **1981**, *85*, 3136.

(9) Zellner, R.; Fritz, B.; Lorenz, K. *J. Atmos. Chem*. **1986**, *4*, 241.

(10) Sehested, J.; Nielson, O. J.; Wallington, T. J. *Chem. Phys. Lett*. **1993**, *213*, 457.

(11) Villalta, P. W.; Huey, L. G.; Howard, C. J. *J. Phys. Chem*. **1996**, *100*, 5808.

(12) Carter, W. P. L.; Atkinson, R. *J. Atmos. Chem.* **1989**, *8*, 165.

(13) Seeley, J. V.; Jayne, J. T.; Molina, M. J. *Int. J. Chem. Kinet*. **1993**, *25*, 571.

(14) Seeley, J. V.; Meads, R. F.; Elrod, M. J.; Molina, M. J. *J. Phys. Chem.* **1996**, *100*, 4026.

(15) Elrod, M. J.; Meads, R. F.; Lipson, J. B.; Seeley, J. V.; Molina, M. J. *J. Phys. Chem.* **1996**, *100*, 5808.

(16) Lipson, J. B.; Elrod, M. J.; Beiderhase, T.; Molina, L. T.; Molina, M. J. *Faraday Trans.* **1997**, *93*, 2665.

(17) DeMore, W. B.; Sander, S. P.; Howard, C. J.; Ravishankara, A. R.; Golden, D. M.; Kolb, C. E.; Hampson, R. F.; Kurylo, M. J.; Molina, M. J. *Chemical Kinetics and Photochemical Data for Use in Stratospheric Modeling*; JPL Publication 97-4; Jet Propulsion Laboratory: Pasadena, California, 1997.

(18) *Chemistry Webbook* (http://webbook.nist.gov/chemistry); National Institute of Standards and Technology: Gaithersberg, Maryland, 1999.

(19) Cheung, Y.-S.; Li, W.-K. *Chem. Phys. Lett.* **1994**, *223*, 383.

(20) Messer, B. M.; Stielstra, D. E.; Cappa, C. D.; Scholtens, K. W.; Elrod, M. J. In preparation.
(21) Adams, N. G.; Smith, D.; Grief, D. *Int. J. Mass Spectrom. Ion Phys.* **1978**, *26*, 405.
(22) Sunderlin, L. S.; Squires, R. R. *Chem. Phys. Lett.* **1993**, *212*, 307.
(23) Lee, T. J.; Rice, J. E. *J. Am. Chem. Soc.* **1992**, *114*, 8247.
(24) Messer, B. M.; Elrod, M. J. In preparation.
(25) Seeley, J. V. Experimental Studies of Gas-Phase Radical Reactions Using the Turbulent Flow Tube Technique. Ph.D. Thesis, Massachusetts Institute of Technology, 1994.